ISSN 2706-655X Vol. 7, Issue 2: 84-95, DOI: 10.25236/IJFET.2025.070212

A Method for Calculating Spatial Thermal Radiation Damage Thresholds Based on the True Temperature Fields of Explosive Fireballs

Zhentao Wang[1,a], Jingmin Dai[1,b,*]

[1]School of Instrumentation Science and Engineering, Harbin Institute of Technology, Harbin, China
[a]dzwztmail@163.com, [b]dongguasina@163.com
**Corresponding author*

Abstract: *Thermal radiation damage is an important aspect of the comprehensive evaluation of explosives. Continuous enhancement in explosive performance and the development of various new weapons and ammunition have recently raised interest in assessing the thermal radiation damage effects induced by explosive fireballs. The thermal radiation damage threshold is a core parameter that directly influences the assessment of explosive performance and weapon design. However, current calculation methods only lead to single-point thermal radiation damage thresholds at specific distances from a fireball, failing to reflect the spatial distribution characteristics of thermal radiation damage, which constrains the applicability of the thermal radiation damage threshold parameter for the optimization of explosive performance and the development of weapons and ammunition. The paper calculates the spatial thermal radiation damage threshold based on the true temperature field of explosive fireballs, fully accounting for the spatial distribution characteristics of fireballs and the time-dependent nature of spectral emissivity. This research provides a solid theoretical foundation for the comprehensive evaluation of thermal radiation damage effects.*

Keywords: *Thermal radiation damage, true temperature field, explosive fireballs*

1. Introduction

Explosive detonation-induced thermal radiation damage originates from the intense thermal radiation emitted by fireballs. When detonating, combustible materials within the explosive undergo rapid chemical reactions, quickly releasing a large amount of energy and forming a high-temperature and high-pressure fireball. The fireball emerges at the explosion center and rapidly expands into the surrounding space, driven by the shockwave. The reaction energy gradually weakens as the combustible materials are consumed, and the thermal radiation intensity decreases and dissipates in the surrounding air[1-4]. The evolution of explosive fireballs is extremely short, typically lasting only a few milliseconds, and it is challenging but necessary to comprehensively account for both temporal and spatial dynamic evolution characteristics when evaluating thermal radiation damage effects.

Thermal radiation damage induced by explosive fireballs was studied back to World War I. To enhance operational effectiveness, the U.S. military at that time required a real-time assessment of target damage to optimize combat strategies, which drove the development of thermal radiation damage assessment methodologies. Over the decades, the main evaluation approaches have evolved into three categories: static modeling, dynamic modeling, and thermal radiation evaluation methods based on fireball temperature fields.

The static modeling method assumes a fireball is a static body that instantaneously reaches its maximum diameter, height, and thermal radiation energy, and this constant state does not change further; fireball parameters depend solely on the type and mass of combustible materials. However, this approach has often led to unrealistic results, e.g., shorter damage distances than the fireball radius[5-7]. To address this, Baker et al. proposed a more practical static theoretical model in 1983, known as the Baker model, which became widely adopted for calculating idealized thermal radiation damage thresholds, exhibiting satisfactory performance when fireball dynamics are neglected[8]. Although the Baker model corrected the limitations concerning the damage distance, it is still based on static assumptions and fails to reflect the temporal evolution of the fireball.

The dynamic modeling method introduced by Martinsen et al. in 1999 provides a dynamic depiction

ISSN 2706-655X Vol. 7, Issue 2: 84-95, DOI: 10.25236/IJFET.2025.070212

of the fireball's evolution by dividing it into a "growth phase" and a "sustained combustion phase", closely matching the actual behavior of the fireball[9]. Nevertheless, the method relies on assumed fireball parameters, introducing a certain uncertainty in practical applications. Consequently, various pyrometric instruments were developed to capture the realistic dynamic evolution of the fireball.

In 2006, Goroshin et al. developed a three-color optical pyrometer to measure the fireball temperatures of both homogeneous and heterogeneous explosives; the pyrometer featured a dual-stage amplification design, a temperature measurement range from 1500 to 6000 K, a sampling frequency of up to 25 MHz, and a spectral response range from 300 to 800 nm[10]. In 2007, Tarasov et al. designed a fiber-optic remote transmission two-wavelength pyrometer and successfully captured the peak temperature of a PETN explosive fireball at approximately 4100 K, occurring within a 25 - 30 μs window[11]. In 2011, Densmore et al. constructed a high-speed two-wavelength imaging pyrometry system using two Phantom v7.3 high-speed CCD cameras, which employed a colorimetric method to acquire two-dimensional temperature distributions of TNT fireballs[12]. In 2024, Ritchie et al. applied high-speed pyrometry techniques to measure the temperature fields of spherical TNT explosive fireballs ranging from 13 to 165 g and systematically analyzed the relationships among the fireball temperature, diameter, height, and charge mass[13]. The experimental results indicated that the growth and decay rates of fireball parameters were almost symmetrical when the charge mass exceeded 55 g, but they decreased by approximately 50% for charges below 55 g. After normalizing the data over time and space, the fireball evolution under different explosive loading conditions followed consistent patterns.

Despite the ability of high-performance pyrometers to dynamically record the temperature field of explosive fireballs, existing methods for calculating thermal radiation damage thresholds fail to fully exploit the information on the spatial distribution of the temperature field and to comprehensively assess spatial thermal radiation effects, mostly leading to single-point thermal radiation damage thresholds at fixed distances[14]. To address this limitation, we proposed a method for calculating spatial thermal radiation damage thresholds based on the true temperature field data recorded using multispectral radiation pyrometry. This method integrates the fireball parameter data from the true temperature field with factors such as the fireball thermal radiation energy, the geometric view between the fireball and the target, and atmospheric transmissivity, achieving the calculation of thermal radiation damage thresholds across spatial domains. On this basis, the *Q*-evaluation criterion was applied to complete the assessment of the spatial thermal radiation damage effects induced by explosive fireballs, providing a solid theoretical foundation for the optimization of explosive performance and the development of weapons and ammunition.

2. Methodology

The thermal radiation energy emitted by an explosive fireball is the main factor that influences the degree of thermal radiation damage: the higher the thermal radiation energy released, the more severe the damaging effect. However, the damage degree sustained by a target also depends on the spatial relationship between the fireball and the target and the attenuation effects of atmospheric transmission. If the spatial location of the target changes, e.g., its distance from the fireball increases, the thermal radiation energy attenuates during propagation, and the target experiences a less energetic thermal wave.

To address this issue, we focused on the computation of the spatial thermal radiation damage thresholds of explosive fireballs and conducted an in-depth analysis from the following aspects: (1) the thermal radiation energy of the fireball; (2) the geometric view factors between the fireball and the target; and (3) the attenuation of thermal radiation energy during propagation. A mathematical expression for calculating thermal radiation damage thresholds by considering these three factors is given as follows:

$$Q = \int_0^{t_{end}} E(t) \cdot F(x) \cdot \tau(x) dt \tag{1}$$

where $E(t)$ is the thermal radiation energy of the explosive fireball, W/m²; F(x) is the geometric view factor between the fireball and the target; τ(x) is the atmospheric attenuation; tend is the duration of the fireball, s.

2.1. Thermal Radiation Energy of Explosive Fireballs

The true temperature field of an explosive fireball can be determined using multispectral radiation pyrometry, facilitating the calculation of the fireball's thermal radiation energy[15]. The following parameters are defined: the true temperature of a fireball, $T(t)$, and the spectral emissivity, $\varepsilon(\lambda, T(t))$; let

ISSN 2706-655X Vol. 7, Issue 2: 84-95, DOI: 10.25236/IJFET.2025.070212

λ_a and λ_b denote the minimum and maximum wavelengths measurable by the instrument, respectively. Based on Planck's law, the thermal radiation flux of a fireball can be expressed as follows:

$$E(t)=\int_{\lambda_a}^{\lambda_b}\varepsilon\left(\lambda,T(t)\right)\cdot\frac{C_1}{\lambda^5\cdot e^{C_2/\lambda T(t)}}d\lambda \tag{2}$$

where C_1 = 3.742×10^{-16} W·m^2, and C_2 = 1.4388×10^{-2} m·K are the first and the second radiation constants of Planck's law, respectively. The true temperature of the explosive fireball in Eq. (2) generally requires inversion from the measured multispectral data following the previously reported account [16]. During the inversion process, the spectral emissivity model is established as follows:

$$\varepsilon(\lambda)=\sum_{k=1}^{m}a_k\lambda^v \quad m\le n-2,-n\le v\le n \tag{3}$$

where n is the number of channels in the multispectral measurement instrument. Eq. (3) describes the spectral emissivity model at a fixed time. To substitute it in Eq. (2), a time parameter must be introduced. The method proposed here integrates the true temperature of an explosive fireball with the spectral emissivity model. By incorporating the temporal evolution of the true temperature, the model assesses the temporal variation of spectral emissivity.

To include the true temperature in the spectral emissivity model, the mathematical relationship between the true temperature and wavelength must be considered. Since the true temperature and wavelength differ in dimensional units, direct addition or subtraction is not feasible, so they must be correlated by multiplication or division using one of the possible mathematical relations: λT, λ/T, or T/λ. Typically, the wavelength range selected for the multispectral characterization of explosive fireballs is between the visible and near-infrared regions, and the values are generally below 1 μm. In contrast, the true temperature of explosive fireballs often exceeds 2000 °C. Under such conditions, λ/T and T/λ approach extremely small or large values, easily causing numerical instability, and negatively affecting the accuracy of model representation, so these relationships are excluded from further analysis. Instead, multiplication is adopted as the mathematical relationship between the true temperature and wavelength, and the spectral emissivity model can be further revised as follows:

$$\varepsilon(\lambda,T)=\sum_{k=1}^{m}b_k\left(\lambda T\right)^v \quad m\le n-2,-n\le v\le n \tag{4}$$

where b_k is the parameter that needs to be determined. The temporal evolution of the true temperature of an explosive fireball can be expressed as a cubic polynomial:

$$T(t)=c_0+c_1t+c_2t^2+c_3t^3 \tag{5}$$

where c_0, c_1, c_2, and c_3 are fitting parameters; t is the duration of the explosive fireball, s. Combining Eqs. (4) and (5) yields a time-dependent model of spectral emissivity for the explosive fireball:

$$\varepsilon\left[\lambda,T(t)\right]=\sum_{k=1}^{m}b_k\left[\lambda\cdot\left(c_0+c_1t+c_2t^2+c_3t^3\right)\right]^v \quad m\le n-2,-n\le v\le n \tag{6}$$

where the fitting parameters c_0, c_1, c_2, and c_3 can be obtained by fitting the true temperature vs. time curve. The b_k parameter must be determined by constructing a system of equations based on multispectral measurement data and the brightness temperature equation expressed as follows:

$$\frac{1}{T}-\frac{1}{T_{\lambda_i}}=\frac{\lambda_i}{C_2}\ln\varepsilon(\lambda_i,T) \tag{7}$$

The brightness temperature equation is a fundamental formula in radiation thermometry, linking temperature, wavelength, and spectral emissivity. In Eq. (7), $T_{\lambda i}$ represents the brightness temperature at a given measurement wavelength λ_i, and it can be directly computed from multispectral measurements using blackbody calibration. Multispectral pyrometers can synchronously acquire brightness temperatures across multiple wavelength channels. Based on the measured brightness temperatures and Eq. (7), a system of equations can be constructed as follows:

ISSN 2706-655X Vol. 7, Issue 2: 84-95, DOI: 10.25236/IJFET.2025.070212

$$\begin{cases} \dfrac{1}{T(t)}-\dfrac{1}{T_{\lambda_1}}=\dfrac{\lambda_1}{C_2}\ln\left\{\sum_{k=1}^{p}b_k\left[\lambda_1\cdot\left(c_0+c_1t+c_2t^2+c_3t^3\right)\right]^v\right\} \\ \cdots \\ \dfrac{1}{T(t)}-\dfrac{1}{T_{\lambda_1}}=\dfrac{\lambda_1}{C_2}\ln\left\{\sum_{k=1}^{p}b_k\left[\lambda_1\cdot\left(c_0+c_1t+c_2t^2+c_3t^3\right)\right]^v\right\} \\ \cdots \\ \dfrac{1}{T(t)}-\dfrac{1}{T_{\lambda_n}}=\dfrac{\lambda_n}{C_2}\ln\left\{\sum_{k=1}^{p}b_k\left[\lambda_n\cdot\left(c_0+c_1t+c_2t^2+c_3t^3\right)\right]^v\right\} \\ \cdots \\ \dfrac{1}{T(t)}-\dfrac{1}{T_{\lambda_n}}=\dfrac{\lambda_n}{C_2}\ln\left\{\sum_{k=1}^{p}b_k\left[\lambda_n\cdot\left(c_0+c_1t+c_2t^2+c_3t^3\right)\right]^v\right\} \end{cases} \tag{8}$$

where λ_1 - λ_n are the measured wavelengths in the n channels of the multispectral pyrometer; $T_{\lambda 1}$ *and* $T_{\lambda n}$ are the corresponding brightness temperatures. As both parameters are known, the least-squares method can be used to find the optimal solution for b_k. Once the parameters are determined, combining Eqs. (2) and (6) yields:

$$E(t)=\int_{\lambda_a}^{\lambda_b}\sum_{k=1}^{m}b_k\left[\lambda\cdot\left(c_0+c_1t+c_2t^2+c_3t^3\right)\right]^v\cdot\frac{C_1}{\lambda^5\cdot e^{C_2/\lambda T(t)}}d\lambda \tag{9}$$

Eq. (9) indicates that the thermal radiation flux of an explosive fireball is calculated in a specific wavelength interval from λ_a to λ_b. However, the actual thermal radiation flux of a fireball is not confined to a specific wavelength range but spans across the entire spectrum, so it must be integrated over the full wavelength range to accurately calculate the total thermal radiation flux.

In practice, this approach faces a major problem: specifically, full-spectrum multispectral data on explosive fireballs cannot be recorded in outdoor environments, mainly due to two reasons. First, water vapor (H_2O) and carbon dioxide (CO_2) in the atmosphere selectively absorb thermal radiation in specific wavelength ranges, hindering its transmission over the full spectrum. Second, the spectral measurement range of pyrometric instruments is inherently limited, and most pyrometers receive thermal radiation light only at a particular wavelength band. Typically, high-speed CCD cameras and infrared thermal imagers used to monitor explosive fireballs mainly cover the visible to near-infrared spectrum and in the 3–5 μm range, respectively, but neither can achieve full-spectrum measurements, so the acquired data cannot meet the integration requirements over the entire spectrum.

In summary, full-spectrum multispectral data of explosive fireballs cannot be recorded due to limitations in the spectral range of the used instruments and selective absorption by atmospheric gases. To effectively calculate the thermal radiation flux of explosive fireballs over the full spectrum, we assumed that a fireball is a gray body, and then approximated its spectral emissivity at a selected wavelength in the instrument's measurement range as equivalent to the full-spectrum spectral emissivity. Although a certain deviation from actual conditions persists, this approach remains feasible and reasonable under current measurement constraints. The specific computational steps are as follows:

First, Eq. (9) implies that calculating the thermal radiation flux between λ_a and λ_b requires a continuous integration over that wavelength range. According to the integral mean value theorem, Eq. (9) can be rewritten as:

$$E(t)=\sum_{k=1}^{m}b_k\left[\lambda_{e,t}\cdot\left(c_0+c_1t+c_2t^2+c_3t^3\right)\right]^v\int_{\lambda_a}^{\lambda_b}\frac{C_1}{\lambda^5\cdot e^{C_2/\lambda T(t)}}d\lambda \tag{10}$$

where $\lambda_{e,t}$ is the arbitrary wavelength in the range from λ_a to λ_b. At a fixed time point, the spectral emissivity at that wavelength can numerically replace the integration result in Eq. (9), expressed as follows:

$$\begin{aligned} E(t)&=\int_{\lambda_a}^{\lambda_b}\sum_{k=1}^{m}b_k\left[\lambda\cdot\left(c_0+c_1t+c_2t^2+c_3t^3\right)\right]^v\cdot\frac{C_1}{\lambda^5\cdot e^{C_2/\lambda T(t)}}d\lambda \\ &=\sum_{k=1}^{m}b_k\left[\lambda_{e,t}\cdot\left(c_0+c_1t+c_2t^2+c_3t^3\right)\right]^v\int_{\lambda_a}^{\lambda_b}\frac{C_1}{\lambda^5\cdot e^{C_2/\lambda T(t)}}d\lambda \end{aligned} \tag{11}$$

ISSN 2706-655X Vol. 7, Issue 2: 84-95, DOI: 10.25236/IJFET.2025.070212

Throughout the entire duration of the explosive fireball, spectral emissivity values $\lambda_{e,t_1}, \lambda_{e,t_1}, ..., \lambda_{e,t_{end}}$ at different time points, denoted as $\lambda_{e,t}$, can be obtained from the multispectral measurement data. These $\lambda_{e,t}$ values are aggregated, and the median is selected as the representative wavelength at which the corresponding spectral emissivity is treated as the full-spectrum spectral emissivity of the fireball. The expression is given by:

$$\varepsilon(t)=\sum_{k=1}^{m} b_k\left[\lambda_t\cdot\left(c_0+c_1t+c_2t^2+c_3t^3\right)\right]^v \quad m\le n-2,-n\le v\le n,\lambda_a\le\lambda_t\le\lambda_b \tag{12}$$

where λ_t is the selected representative wavelength, μm. Since this full-spectrum spectral emissivity is calculated assuming the fireball is a gray body, its value varies only with time but remains constant with respect to wavelength. Consequently, the thermal radiation energy can be expressed as follows:

$$E(t)=\int_0^{\infty}\varepsilon(t)\cdot\frac{C_1}{\lambda^5\cdot e^{C_2/\lambda T(t)}}d\lambda \tag{13}$$

Applying the Stefan-Boltzmann law to simplify Eq. (13), the expression for the thermal radiation energy of the fireball over the full wavelength range is:

$$E(t)=\varepsilon(t)\cdot\sigma\cdot T^4(t) \tag{14}$$

2.2. Geometric View Factors Between a Fireball and a Target

The geometric view factor between an explosive fireball and a target determines the transmission efficiency of the fireball's thermal radiation energy, which mainly depends on the relative spatial distance between the fireball and the target. This serves as a basis for constructing a three-dimensional Cartesian coordinate system, combining the actual measured true temperature field data of the fireball and the spatial location of the target, Figure 1. This coordinate system allows an independent calculation of the geometric view factor between each fireball surface element and the target from the true temperature field data. Subsequently, the thermal radiation flux from each surface element to the target is derived based on the corresponding thermal radiation energy. Finally, using the additive characteristic of geometric view factors, the total thermal radiation flux from the explosive fireball to the target is obtained.

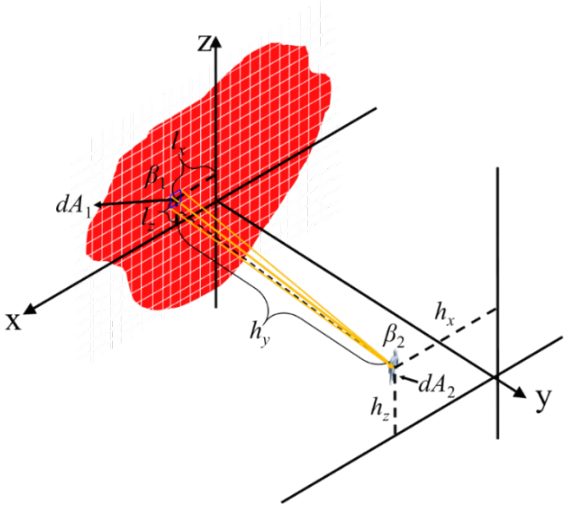

Figure 1 The three-dimensional Cartesian coordinate system between an explosive fireball and a target

In Figure 1, the *xoz* plane represents the projection plane of the explosive fireball in the target direction and corresponds to the measured true temperature field. The center of this plane denotes the explosion initiation point. The actual horizontal and vertical distances from a given surface element with a corresponding true temperature to the explosion center are denoted as l_x and l_z, respectively. The actual horizontal and vertical distances from the target projection to the explosion center are denoted as h_x and h_y, respectively, while h_z represents the vertical distance from the target to the fireball projection plane. The area dA_1 refers to the surface element at a true temperature point, and β_1 is the angle between the target direction and the normal direction of the fireball surface. The area dA_2 represents the surface element on the target, and β_2 is the angle between the fireball's direction and the normal direction of the target surface.

ISSN 2706-655X Vol. 7, Issue 2: 84-95, DOI: 10.25236/IJFET.2025.070212

To calculate l_x and l_z, the actual horizontal and vertical dimensions of each fireball surface element in the true temperature field data must be determined as follows:

$$\begin{cases} w_x = \dfrac{2 \cdot d \cdot \tan\left(\dfrac{x_{fov}}{2}\right)}{x_{pix}} \\ w_z = \dfrac{2 \cdot d \cdot \tan\left(\dfrac{z_{fov}}{2}\right)}{z_{pix}} \end{cases} \tag{15}$$

where x_{fov} and z_{fov} are the field of view angles in the horizontal and vertical directions, respectively, x_{pix} and z_{pix} are the horizontal and vertical resolutions of the true temperature field data, respectively, w_x and w_y are the actual horizontal and vertical sizes of the fireball surface element corresponding to a true temperature point, respectively, and d is the actual measurement distance. For any true temperature point at the coordinate position (n_x, 0, n_z), the corresponding l_x and l_z values can be calculated as:

$$\begin{cases} l_x = n_x \cdot w_x \\ l_z = n_z \cdot w_z \end{cases} \tag{16}$$

If the target coordinates are set as (m_x, m_y, m_z), then referring to the actual size of the fireball surface element, h_x and h_z are given by:

$$\begin{cases} h_x = m_x \cdot w_x \\ h_z = m_z \cdot w_z \end{cases} \tag{17}$$

The h_y value should be determined based on specific needs. Using the above parameters, the actual distance between the fireball surface element and the target surface element, L, can be expressed as:

$$L = \sqrt{\left(h_x - l_x\right)^2 + h_y^2 + \left(h_z - l_z\right)^2} \tag{18}$$

Based on the definition of the geometric view factor, the view factor dF between any two surface elements can be expressed as:

$$dF = \frac{\cos\theta_1 \cos\theta_2}{\pi L^2} dA_2 \tag{19}$$

where θ_1 and θ_2 are the angles between the line connecting the two surface elements and their respective surface normal, respectively. By substituting Eq. (18) into Eq. (19), the geometric view factor between the fireball surface element and the target surface element can be derived as follows:

$$dF = \frac{\cos\theta_1 \cos\theta_2}{\pi\left[\left(h_x - l_x\right)^2 + h_y^2 + \left(h_z - l_z\right)^2\right]} dA_2 \tag{20}$$

According to the thermal radiation energy expression in Eq. (14), the total thermal flux dq_1 from the fireball surface element dA_1 is:

$$dq_1 = E(t) \cdot dA_1 = \varepsilon(t) \cdot \sigma \cdot T^4(t) \cdot dA_1 \tag{21}$$

By combining Eq. (21) with Eq. (20), the thermal radiation energy from a fireball surface element to a target surface element is:

$$d^2 q_{dA_1 \to dA_2} = \varepsilon(t) \cdot \sigma T^4(t) \cdot \frac{\cos\theta_1 \cos\theta_2}{\pi\left[\left(h_x - l_x\right)^2 + h_y^2 + \left(h_z - l_z\right)^2\right]} dA_1 dA_2 \tag{22}$$

Integrating Eq. (22) over both the fireball A_1 and the target A_2 yields the thermal radiation energy received by the target from the explosive fireball:

$$q_{A_1 \to A_2} = \int_{A_1} \int_{A_2} \varepsilon(t) \cdot \sigma T^4(t) \cdot \frac{\cos\theta_1 \cos\theta_2}{\pi\left[\left(h_x - l_x\right)^2 + h_y^2 + \left(h_z - l_z\right)^2\right]} dA_1 dA_2 \tag{23}$$

ISSN 2706-655X Vol. 7, Issue 2: 84-95, DOI: 10.25236/IJFET.2025.070212

Further integrating Eq. (23) over time gives:

$$Q_{A_1 \to A_2} = \int_0^{t_{end}} \int_{A_1} \int_{A_2} \varepsilon(t) \cdot \sigma T^4(t) \cdot \frac{\cos\theta_1 \cos\theta_2}{\pi\left[(h_x - l_x)^2 + h_y^2 + (h_z - l_z)^2\right]} dA_1 dA_2 dt \tag{24}$$

where $Q_{A_1 \to A_2}$ is the total thermal radiation energy received by the target during the entire explosive fireball duration. Based on Eq. (24) and neglecting the atmospheric attenuation, the total thermal radiation energy that a target receives within the thermal radiation damage region of an explosive fireball can be theoretically calculated.

2.3. Calculation of Atmospheric Attenuation

Atmospheric attenuation represents the reduction in the explosive fireball thermal radiation energy during its propagation through the atmosphere. It originates from gas molecules that absorb a part of thermal energy, and particular emphasis is placed on water vapor and carbon dioxide in studies of thermal radiation damage effects caused by explosive fireballs. To quantitatively describe this effect, we adopted the atmospheric attenuation expression from Ref. [17]:

$$\begin{aligned} \tau(x,t) = 1.006 - 0.1171\lg\left(X_{H_2O}\right) - 0.02368\left[\lg\left(X_{H_2O}\right)\right]^2 \\ - 0.03188\lg\left(X_{CO_2}\right) + 0.001164\left[\lg\left(X_{CO_2}\right)\right]^2 \end{aligned} \tag{25}$$

where X_{CO_2} and X_{H_2O} are the thermal energy absorption rates of carbon dioxide and water vapor in the atmosphere, respectively. The calculation of these absorption rates incorporates the spatial relationship between the explosive fireball and the target, using the following expressions:

$$X_{H_2O} = \frac{2.165}{T_a} \ln(RH) P_V \sqrt{(h_x - l_x)^2 + h_y^2 + (h_z - l_z)^2} \tag{26}$$

$$X_{CO_2} = \frac{273}{T_a} \ln\left(\sqrt{(h_x - l_x)^2 + h_y^2 + (h_z - l_z)^2}\right) \tag{27}$$

where RH is the relative humidity (%) at ambient temperature, P_V is the saturation vapor pressure of water (Pa) at ambient temperature, and T_a is the ambient temperature (K). Substituting Eqs. (26) and (27) into Eq. (25), and combining it with the expression in Eq. (1) and then linking with Eq. (24), the calculated thermal radiation damage threshold of an explosive fireball to an arbitrary target in its damage-effective space (with atmospheric attenuation considered) is as follows:

$$\begin{aligned} Q &= \tau(x) \cdot Q_{A_1 \to A_2} \\ &= \int_0^{t_{end}} \int_{A_1} \int_{A_2} \tau(x) \cdot \varepsilon(t) \cdot \sigma T^4(t) \cdot \frac{\cos\theta_1 \cos\theta_2}{\pi\left[(h_x - l_x)^2 + h_y^2 + (h_z - l_z)^2\right]} dA_1 dA_2 dt \end{aligned} \tag{28}$$

Based on Eq. (28), by incorporating the true temperature field data of the explosive fireball and the spatial location of the target, the required spatial thermal radiation damage threshold can be calculated. This analytical solution provides a solid theoretical basis for evaluating the spatial thermal radiation damage effects of explosive fireballs.

3. Methodology

The effectiveness of the proposed method was experimentally verified on TNT explosive fireballs. The procedure involved three main stages: first, experiments were conducted to measure the true temperature field; second, the measured data were used to compute the spatial thermal radiation damage thresholds of explosive fireballs; and third, the thermal radiation damage effects were evaluated based on the thermal dose evaluation criterion.

ISSN 2706-655X Vol. 7, Issue 2: 84-95, DOI: 10.25236/IJFET.2025.070212

3.1. Measurement of the True Temperature Field of TNT Explosive Fireballs

Before the experiment, the explosive samples were securely fixed on a wooden tripod to lock in their positions during detonation. The multispectral pyrometric instrument was placed outside the fireball's damage radius, and the lens was adjusted to ensure a clear image of the sample appearing on the computer screen. To warrant absolute operational safety, a protective barrier wall was raised upright at the test site, and the pyrometer remotely measured the explosive fireball through a viewing window in the barrier. Figure 2 shows the experimental setup at the test site, while Figure 3 presents the true temperature field images of the TNT explosive fireball. The technical specifications of the multispectral pyrometer used in this study are listed in Table 1, and a detailed structural design is given in Ref. [18].

Figure 2 The experimental setup for measuring a TNT explosive fireball

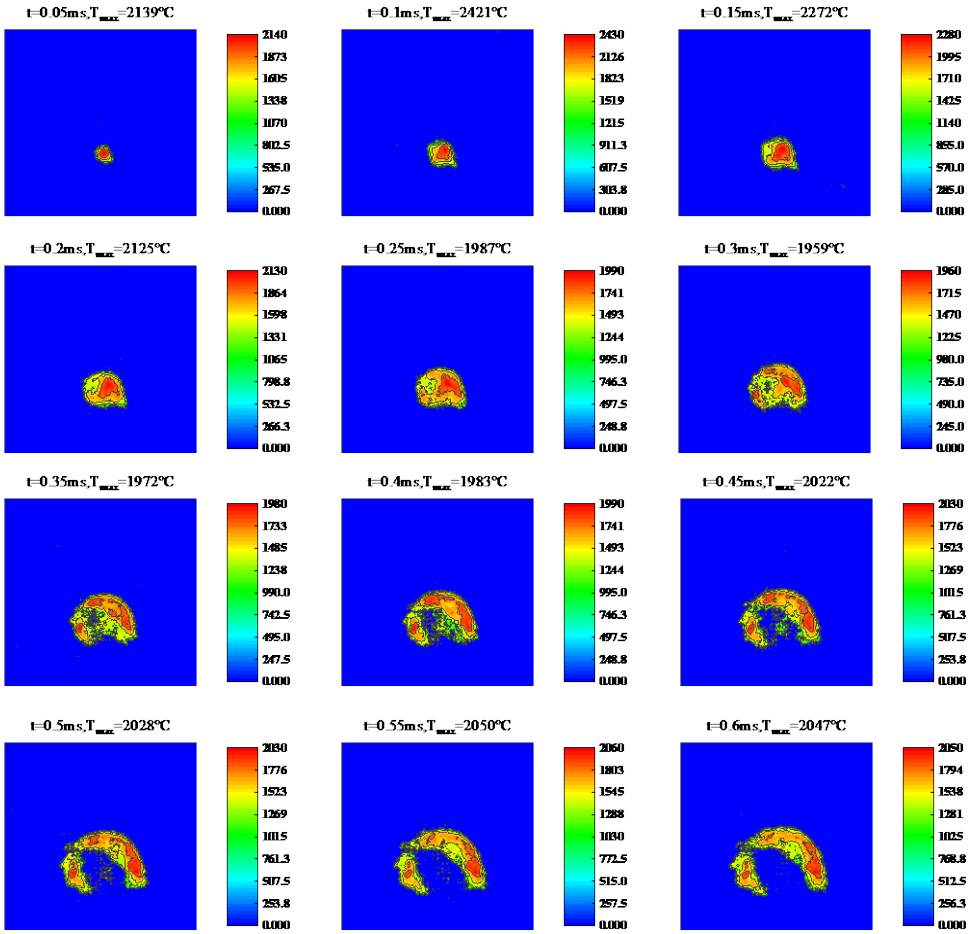

Figure 3 True temperature field images of a TNT explosive fireball

ISSN 2706-655X Vol. 7, Issue 2: 84-95, DOI: 10.25236/IJFET.2025.070212

Table 1 Technical specifications of the multispectral pyrometric instrument

Specification	Value
Temperature measurement range	1500 - 2700 ℃
Spectral range	0.4 - 1.1μm
Maximum sampling rate	20000 fps
True temperature uncertainty	≤ 3 %
Number of wavelengths	Four
Measurement distance	100 - 150 m

As shown in Figure 3, the TNT explosive fireball rapidly expands outward from the explosion center immediately after detonation. At 0.35 ms, the central region of the fireball starts to dissipate. Driven by the shockwave, this dissipation intensifies, though the overall fireball retains an elliptical shape. At 0.5 ms, the central fireball is fully dissipated, having only the peripheral flames still burning. At this point, a distinct asymmetry becomes apparent: the combustion region is significantly larger on the right than on the left side. After 0.6 ms, approximately half of the left-side flame is dissipated, while the right-side flame also begins to weaken due to the air layer thickening. Throughout the process, the TNT fireball consistently expands horizontally, retaining morphologically a relatively regular elliptical structure in its early stage; despite the central dissipation, its overall shape remains stable without significant deformation.

3.2. Calculation of the Spatial Thermal Radiation Damage Threshold of TNT Explosive Fireballs

In this experiment, the spatial thermal radiation damage thresholds were calculated using the measured true temperature field data of the TNT fireball by applying the proposed method. Figure 4 illustrates the planar distribution of thermal radiation damage from the TNT explosive fireball within a range of 5 - 10 m.

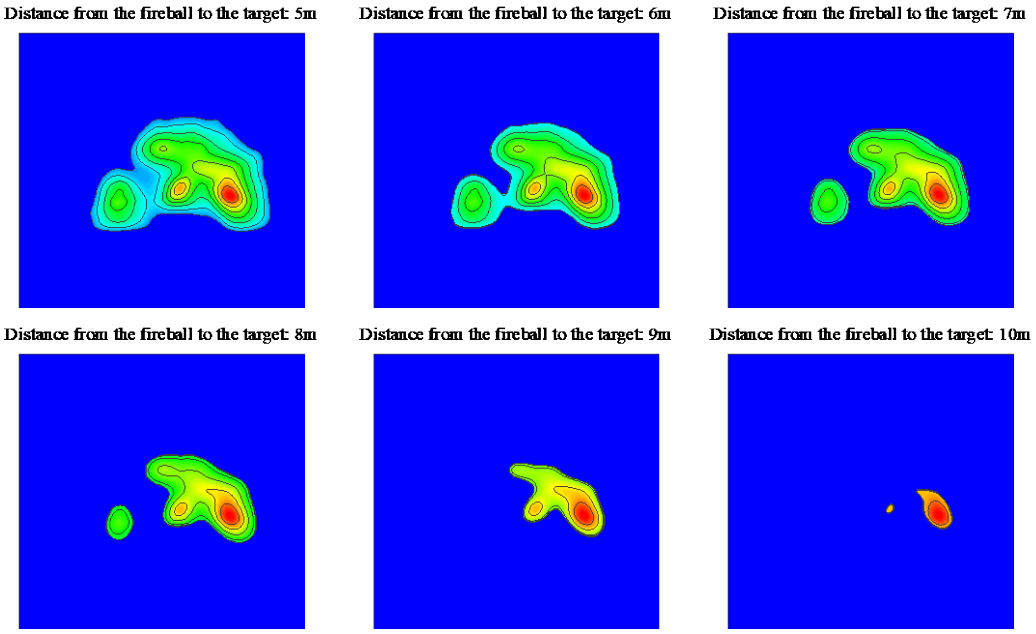

Figure 4 The planar thermal radiation damage distribution of a TNT explosive fireball

The thermal radiation damage effects of the TNT explosive exhibit a distinct left-right separation, becoming increasingly obvious with distance. When the target is placed 7 m from the fireball, the damage zones on the left and right sides are segregated; when the distance is further increased to 9 m, the right-side damage region almost entirely vanishes. To depict the spatial distribution characteristics of thermal radiation damage more intuitively, the planar damage maps at different distances are integrated to form a spatial distribution map, Figure 5.

ISSN 2706-655X Vol. 7, Issue 2: 84-95, DOI: 10.25236/IJFET.2025.070212

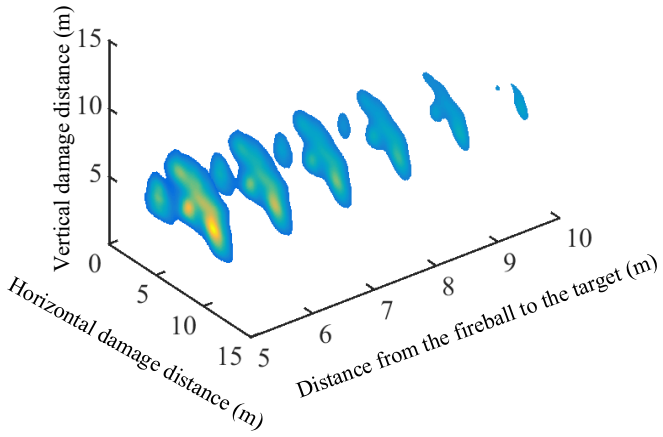

Figure 5 The spatial thermal radiation damage distribution of a TNT explosive fireball

3.3. Evaluation of the Thermal Radiation Damage Effects from TNT Explosive Fireballs

To comprehensively assess the range of thermal radiation damage effects caused by TNT explosive fireballs, horizontal and vertical damage distances were derived based on the thermal radiation damage thresholds specified in the thermal dose evaluation criterion. Table 2 lists the thermal radiation damage thresholds and corresponding effects according to the thermal dose criterion, while detailed evaluation results are provided in Table 3.

Table 2: Thermal radiation damage thresholds and corresponding effects based on the thermal dose evaluation criterion

Criterion	Thermal radiation damage threshold / kJ/m^2	Thermal radiation damage effects
Thermal dose criterion	592	Fatality
	375	Third-degree burns
	172	Minor burns
	65	Skin pain

Table 3: Horizontal and vertical thermal radiation damage distances of a TNT explosive fireball

Distance	Thermal radiation damage effect	TNT explosive	
		Horizontal damage distance	Vertical damage distance
5 m	Fatality	2.15 m	1.95 m
	Third-degree burns	6.75 m	4.50 m
	Minor burns	9.05 m	5.90 m
	Skin pain	9.40 m	6.20 m
6 m	Fatality	0.40 m	0.45 m
	Third-degree burns	4.70 m	3.60 m
	Minor burns	8.60 m	5.50 m
	Skin pain	8.85 m	5.75 m
7 m	Fatality	-	-
	Third-degree burns	2.10 m	2.00 m
	Minor burns	8.30 m	5.25 m
	Skin pain	8.35 m	5.30 m
8 m	Fatality	-	-
	Third-degree burns	0.95 m	1.10 m
	Minor burns	7.15 m	4.75 m
	Skin pain	7.20 m	4.80 m
9 m	Fatality	-	-
	Third-degree burns	-	-
	Minor burns	4.95 m	3.90 m
	Skin pain	5.00 m	3.95 m
10 m	Fatality	-	-
	Third-degree burns	-	-
	Minor burns	2.20 m	2.00 m
	Skin pain	2.25 m	2.10 m

ISSN 2706-655X Vol. 7, Issue 2: 84-95, DOI: 10.25236/IJFET.2025.070212

As shown in Table 3, the range of thermal radiation damage from TNT explosions decreases with distance. When fatality is used as the evaluation criterion, the horizontal and vertical damage distances at 5 m are 2.15 and 1.95 m, respectively. However, beyond 7 m, the thermal radiation dose is no longer sufficient to cause fatality but induces third-degree burns. At a distance of 10 m, the thermal radiation damage effect further weakens, potentially causing only minor burns. The corresponding horizontal and vertical damage distances are 2.20 and 2.00 m, respectively.

4. Conclusion

We proposed a novel method for calculating the spatial thermal radiation damage thresholds of TNT explosive fireballs, consisting of three components: (1) the thermal radiation energy of the fireball is computed based on Planck's law by accounting for the true temperature and the time-dependent nature of spectral emissivity; (2) the geometric relationship between the fireball and the target is incorporated by calculating the geometric view factors between corresponding surface elements of the fireball and the target and then their integration to obtain the total view factor; (3) atmospheric attenuation caused by water vapor and carbon dioxide is computed for each spatial location. The integration of these factors leads to a theoretical formula for calculating spatial thermal radiation damage thresholds.

Using the proposed method, we computed the spatial thermal radiation damage thresholds for TNT explosive fireballs and generated the corresponding damage distribution map. The main results show that, at a distance of 5 m, the horizontal and vertical damage distances leading to fatal injuries are 2.15 and 1.95 m, respectively. At 10 m, the thermal radiation emitted by the TNT explosive fireball is no longer lethal and causes only minor burns, with the corresponding horizontal and vertical damage distances of 2.20 and 2.00 m, respectively. These findings validate the effectiveness of the proposed method in assessing the effects of spatial thermal radiation damage.

Acknowledgements

This research is funded by the Youth Science Fund Project (Grant No. 62305053).

References

[1] R Shi, G Fang, C Qiao, et al. Investigation into the gel substrate fabrication of a novel ammonium amine explosive and its generic properties exploration [J]. Colloids and Surfaces A: Physicochemical and Engineering Aspects, 2024, 682: 132918.

[2] L Zhang, X Li, S Wang, et al. Facile energetic fluoride chemistry induced organically coated aluminum powder with effectively improved ignition and combustion performances[J]. Journal of thermal analysis and calorimetry, 2023, 148(13): 5957-5966.

[3] YR Li, H Ren, XZ Wu, et al. Estimating energy release performance of oxidizer-activated aluminum fuel particles under ultrafast stimulus[J]. Defence Technology, 2023, 23(5): 92-99.

[4] YK Wang, CG Zhu, D Liu.Effect of Al–Mg–Mn Alloy on the Ignition Performance of RDX, HMX and CL-20[J]. Science of Advanced Materials, 2022,14(2): 350-360.

[5] AF Roberts. Thermal radiation hazards from releases of LPG from pressurised storage[J]. Fire Safety Journal, 1982, 4(3): 197-212.

[6] SB Dorofeev, VP Sidorov, AA Efimenko, et al. Fireballs from deflagration and detonation of heterogeneous fuel-rich clouds[J]. Fire Safety Journal, 1995, 25(4): 323-336.

[7] RW High. The Saturn Fireball[J]. Annals of the New York Academy of Sciences, 1968, 152(1): 441-451.

[8] WE Baker, AP Cox, PS westine, et al. Explosion hazards and evaluation[M]. Elsevier: Elsevier Science Pub Co, 1983.

[9] Martinsen W E, Marx J. An imprvoed model for the prediction of radiant heat rom fireballs[C]//1999 International Conference and Workshop on Modeling Consequences of Accidental Releases of Hazardous Materials San Francisco, 1999.

[10] Goroshin S, Frost D L, Levine J, et al. Optical pyrometry of fireballs of metalized explosives[J]. WILEY-VCH Verlag GmbH & Co. KGaA, 2006, 31(3): 169-180.

[11] MD Tarasov, II Karpenko, VA Sudovtsov, et al. Measuring the brightness emperature of a detonation front in a porous explosive[J]. Combustion, Explosion, and Shock Waves, 2007, 43(4): 465-467.

[12] JM Densmore, BE Homan, MM Biss, et al. High-speed two-camera imaging pyrometer for mapping

ISSN 2706-655X Vol. 7, Issue 2: 84-95, DOI: 10.25236/IJFET.2025.070212

fireball temperatures[J]. Applied Optics, 2011, 50(33): 6267-6271.
[13] Cole Ritchie, Steven W Dean, Kevin L McNesby, et al. Thermal behavior of explosive fireballs as a function of charge size[J]. Research article, 2024, (1): 1:8.
[14] JA Vílchez, M Muñoz, JM Bonilla, et al. Configuration factors for ground level fireballs with shadowing[J]. Journal of Loss Prevention in the Process Industries, 2018, (51): 169-177.
[15] Wang K , Liu Z , Qian X ,et al.Comparative Study on Blast Wave Propagation of Natural Gas Vapor Cloud Explosions in Open Space Based on a Full-Scale Experiment and PHAST[J].Energy & Fuels, 2016, (30): 6143-6152.
[16] ZT Wang, JM Dai. Multi-spectral radiation thermometry based on the reconstructed spectral emissivity model[J]. Measurement, 2024,(288):114346.
[17] Pani KR. LNG fires: A review of experimental results, models and hazard prediction chanllenges[J]. Journal of Hazaedous Materials, 2007, (140): 444-464.
[18] ZT Wang, JM Dai, Yang S. The development of a multispectral pyrometer for achievable true temperature field measurements of the explosion flame[J].Measurement Science & Technology, 2023, (34): 065501.